

# Experimental $(n,\gamma)$ cross sections of the $p$ -process nuclei $^{74}\text{Se}$ and $^{84}\text{Sr}$

I. Dillmann,\* M. Heil, and F. Käppeler

*Institut für Kernphysik, Forschungszentrum Karlsruhe, Postfach 3640, D-76021 Karlsruhe, Germany*

T. Rauscher and F.-K. Thielemann

*Departement Physik und Astronomie, Universität Basel,*

*Klingelbergstrasse 82, CH-4056 Basel, Switzerland*

(Dated: November 8, 2018)

The nucleosynthesis of elements beyond iron is dominated by the  $s$  and  $r$  processes. However, a small amount of stable isotopes on the proton-rich side cannot be made by neutron capture and are thought to be produced by photodisintegration reactions on existing seed nuclei in the so-called “ $p$  process”. So far most of the  $p$ -process reactions are not yet accessible by experimental techniques and have to be inferred from statistical Hauser-Feshbach model calculations. The parametrization of these models has to be constrained by measurements on stable proton-rich nuclei. A series of  $(n,\gamma)$  activation measurements, related by detailed balance to the respective photodisintegrations, were carried out at the Karlsruhe Van de Graaff accelerator using the  $^7\text{Li}(p,n)^7\text{Be}$  source for simulating a Maxwellian neutron distribution of  $kT=25$  keV. First results for the experimental  $(n,\gamma)$  cross sections of the light  $p$  nuclei  $^{74}\text{Se}$  and  $^{84}\text{Sr}$  are reported. These experimental values were used for an extrapolation to the Maxwellian averaged cross section at 30 keV,  $\langle\sigma\rangle_{30}$ , yielding  $271\pm 15$  mb for  $^{74}\text{Se}$ , and  $300\pm 17$  mb for the total capture cross section of  $^{84}\text{Sr}$ . The partial cross section to the isomer in  $^{85}\text{Sr}$  was found to be  $190\pm 10$  mb.

PACS numbers: 25.40.Lw, 26.30.+k, 27.50.+e, 97.10.Cv

## I. INTRODUCTION

Astrophysical models can explain the origin of most nuclei beyond the iron group in a combination of processes involving neutron captures on long ( $s$  process) or short ( $r$  process) time scales [1, 2]. However, 32 stable, proton-rich isotopes between  $^{74}\text{Se}$  and  $^{196}\text{Hg}$  cannot be formed in that way. Those  $p$  nuclei are 10 to 100 times less abundant than the  $s$  and  $r$  nuclei in the same mass region. They are thought to be produced in the so-called  $\gamma$  or  $p$  process, where proton-rich nuclei are made by sequences of photodisintegrations and  $\beta^+$  decays [3, 4, 5]. In this scenario, pre-existing seed nuclei from the  $s$  and  $r$  processes are destroyed by photodisintegration in a high-temperature environment, and proton-rich isotopes are produced by  $(\gamma,n)$  reactions. When  $(\gamma,p)$  and  $(\gamma,\alpha)$  reactions become comparable or faster than neutron emission within an isotopic chain, the reaction path branches out and feeds nuclei with lower charge number  $Z$ . The decrease in temperature at later stages of the  $p$  process leads to a freeze-out via neutron captures and mainly  $\beta^+$  decays, resulting in the typical  $p$ -process abundance pattern with maxima at  $^{92}\text{Mo}$  ( $N=50$ ) and  $^{144}\text{Sm}$  ( $N=82$ ).

The currently most favored astrophysical site for the  $p$  process is explosive burning in type II supernovae. The explosive shock front heats the outer O/Ne shell of the progenitor star to temperatures of 2-3 GK, sufficient for

providing the required photodisintegrations. Following the nucleosynthesis in such astrophysical models, good agreement with the required  $p$  production is found, with exception of the low ( $A<100$ ) and intermediate ( $150\leq A\leq 165$ ) mass range, which are underproduced by factors of 3-4 [6]. Because of these persisting problems, alternative scenarios (such as type Ia supernovae and X-ray bursters) have been suggested, each with their own, inherent difficulties [7, 8, 9]. Currently, however, it is not yet clear whether the observed underproductions are due to a problem with astrophysical models or with the nuclear physics input, i.e. reaction rates. Thus, a necessary requirement towards a consistent understanding of the  $p$  process is the reduction of uncertainties in nuclear data. By far most of the several hundreds of required photodisintegration rates and their inverses need to be inferred from Hauser-Feshbach statistical model calculations [10], e.g. the codes NON-SMOKER [11, 12, 13] and MOST [14, 15]. Experimental data can improve the situation in two ways, either by directly replacing predictions with measured cross sections in the relevant energy range, or by testing the reliability of predictions at other energies when the relevant energy range is not experimentally accessible.

The role of  $(n,\gamma)$  reactions in the  $p$  process was underestimated for a long time, although it is obvious that they have an influence on the final  $p$ -process abundances. Neutron captures compete with  $(\gamma,n)$  reactions and thus hinder the photodisintegration flux towards light nuclei, especially at lower- $Z$  isotopes and even-even isotopes in the vicinity of branching-points. The influence of a variation of reaction rates on the final  $p$  abundances has

---

\*Electronic address: iris.dillmann@ik.fzk.de; also at Departement für Physik und Astronomie, Universität Basel.

been studied previously [16, 17]. It turned out that the  $p$  abundances are very sensitive to changes of the neutron-induced rates in the entire mass range, whereas the proton-induced and  $\alpha$ -induced reaction rates are important at low and high mass numbers, respectively.

Rayet et al. [18] have also studied the influence of several components in their  $p$ -process network calculations. Their nuclear flow schemes show that branching points occur even at light  $p$  nuclei, and are shifted deeper into the proton-rich unstable region with increasing mass and temperature. In contradiction to Woosley and Howard [3], who claimed for their network calculations that  $(n,\gamma)$  can be neglected except for the lightest nuclei ( $A \leq 90$ ), Rayet et al. also examined the influence of neutron reactions for temperatures between  $T_9 = 2.2$  and  $3.2$  GK by comparing overabundance factors if  $(n,\gamma)$  reactions on  $Z > 26$  nuclides are considered or completely suppressed. As a result, the overabundances were found to change by up to a factor 100 (for  $^{84}\text{Sr}$ ) if the  $(n,\gamma)$  channel was artificially suppressed. This rather high sensitivity indicates the need for reliable  $(n,\gamma)$  rates to be used in  $p$ -process networks.

Although recent efforts are directed to calculation or measurement of photodisintegration cross sections and rates [19, 20, 21, 22, 23, 24, 25], astrophysical photodisintegration rates can easily be inferred from capture rates by detailed balance, even in theoretical work [12]. The stellar reaction rate  $N_A \langle \sigma v \rangle_{n,\gamma}^*$  for the reaction  $a + n \rightarrow b + \gamma$  is related to its inverse rate by

$$N_A \langle \sigma v \rangle_{\gamma,n}^* = \frac{(2J_a + 1)(2J_n + 1)}{2J_b + 1} \sqrt{\left(\frac{A_a}{A_b}\right)^3} \times \\ \times \frac{G_a(T)}{G_b(T)} \exp\left(-\frac{Q_{n,\gamma}}{kT}\right) N_A \langle \sigma v \rangle_{n,\gamma}^* \quad (1)$$

with the Avogadro number  $N_A$ , the nuclear spins  $J$  and masses  $A$ , the respective temperature-dependent partition functions  $G(T)$  and the reaction  $Q$  value in the exponent. Measuring or calculating a rate in the direction of positive  $Q$  value ensures best numerical accuracy and consistency between forward and backward reaction. This is important when implementing those rates in reaction networks for nucleosynthesis models.

Moreover, stellar cross sections and rates have to be employed for the computation of reverse rates. In a stellar environment, nuclei are fully thermalized with the environment, resulting in a thermal excitation of both the target and the final nucleus. Only stellar cross sections including the excitation in form of a stellar enhancement factor (SEF) can be used to properly account for all transitions when applying detailed balance. For reactions with positive  $Q$  values for captures, a laboratory measurement of the capture cross section will encompass by far more of the relevant transitions than a photodisintegration experiment, even with the target being in the ground state [20].

For the past decade there has been a continuing effort to measure nuclear data for the  $p$  process, both for

charged particle reactions [17, 26, 27, 28, 29, 30, 31, 32, 33, 34, 35, 36, 37, 38] and for neutron induced reactions [17, 35, 39, 40, 41]. The present work comprises the first measurement of  $(n,\gamma)$  cross sections for the  $p$ -process isotopes  $^{74}\text{Se}$  and  $^{84}\text{Sr}$  at  $kT = 25$  keV, with the aim to improve the  $p$ -process database and to help testing theoretical predictions. Since it is not possible to measure cross sections directly at  $p$ -process temperatures of  $kT = 170$ - $260$  keV, we have to perform the measurements at  $s$ -process (and freeze-out) temperatures of  $kT = 25$  keV, and then extrapolate theoretically by means of the respective energy dependent cross sections (see Sec. V).

The measurement of stellar  $(n,\gamma)$  rates requires a "stellar" neutron source yielding neutrons with a Maxwell-Boltzmann energy distribution. We achieve this by making use of the  $^7\text{Li}(p,n)^7\text{Be}$  reaction. In combination with the activation or time-of-flight technique, this offers a unique tool for comprehensive studies of  $(n,\gamma)$  rates and cross sections for astrophysics.

In Sec. II, the experimental technique and sample characteristics are outlined, followed by the description of the data analysis in Sec. III. The results are presented in Sec. IV. A comparison to theory and extrapolation to higher energies is given in Sec. V. The paper is concluded with a summary and a short outlook in Sec. VI.

## II. EXPERIMENTAL TECHNIQUE

All measurements were carried out at the Karlsruhe 3.7 MV Van de Graaff accelerator using the activation technique. Neutrons were produced with the  $^7\text{Li}(p,n)^7\text{Be}$  source by bombarding  $30 \mu\text{m}$  thick layers of metallic Li on a water-cooled Cu backing with protons of 1912 keV, 30 keV above the reaction threshold. The resulting quasi-stellar neutron spectrum approximates a Maxwellian distribution for  $kT = 25.0 \pm 0.5$  keV [42]. Hence, the proper stellar capture cross section can be directly deduced from our measurement.

For the activations natural samples of selenium metal (0.89%  $^{74}\text{Se}$ ) and various strontium compounds (0.56%  $^{84}\text{Sr}$ ) were used. In order to verify the stoichiometry, samples of  $\text{Sr}(\text{OH})_2$  and  $\text{SrF}_2$  were dried at  $300^\circ\text{C}$  and  $800^\circ\text{C}$ , respectively. The powders were pressed to thin pellets, which were enclosed in a  $15 \mu\text{m}$  thick aluminium foil and sandwiched between  $10$ - $30 \mu\text{m}$  thick gold foils of the same diameter. In this way the neutron flux can be determined relative to the well-known capture cross section of  $^{197}\text{Au}$  [42]. The activation measurements were carried out with the Van de Graaff accelerator operated in DC mode with a current of  $\approx 100 \mu\text{A}$ . The mean neutron flux over the period of the activations was  $\approx 1.5 \times 10^9$   $n/s$  at the position of the samples, which were placed in close geometry to the Li target. Throughout the irradiation the neutron flux was recorded in intervals of 1 min using a  $^6\text{Li}$ -glass detector for later correction of the number of nuclei, which decayed during the activation (factor  $f_b$  in Eq. 4).

Over the course of the present measurements, a total of 17 activations (5 for Se and 12 for Sr) have been carried out with modified experimental parameters (see Table I). Five short-time activations of 3 h to 5 h were used for determining the partial cross section of the  $^{84}\text{Sr}(n,\gamma)^{85}\text{Sr}^m$  reaction feeding the isomer in  $^{85}\text{Sr}$  with a half-life of 67.6 m. The  $^{84}\text{Sr}(n,\gamma)^{85}\text{Sr}^g$  cross section to the ground state was separately deduced from seven long-time activations.

TABLE I: Activation schemes and sample characteristics. The suffix "m" denotes short time activations for measurements of the partial cross section to the  $^{85}\text{Sr}^m$  isomeric state.  $\Phi_{tot}$  gives the neutron exposure of the sample during the activation.

Sample No.	$\varnothing$ [mm]	Mass [mg]	Atoms $^{74}\text{Se}$ or $^{84}\text{Sr}$	$t_a$ [h]	$\Phi_{tot}$ [neutrons]
<b>Se</b>					
se-1	6	151.8	$1.03 \times 10^{19}$	16	$1.10 \times 10^{14}$
se-2	10	200.2	$1.36 \times 10^{19}$	7	$1.53 \times 10^{13}$
se-3	6	102.2	$6.94 \times 10^{18}$	23	$1.64 \times 10^{14}$
se-4	10	207.8	$1.41 \times 10^{19}$	24	$0.99 \times 10^{14}$
se-5	10	147.8	$1.00 \times 10^{19}$	24	$1.16 \times 10^{14}$
<b>Sr(OH)<sub>2</sub></b>					
sr-1	6	67.6	$1.88 \times 10^{18}$	23	$1.45 \times 10^{14}$
sr-2	10	161.2	$4.47 \times 10^{18}$	25	$8.03 \times 10^{13}$
sr-3 <sup>a</sup>	6	119.8	$3.32 \times 10^{18}$	21	$1.59 \times 10^{14}$
sr-4m	6	147.5	$4.09 \times 10^{18}$	3	$1.13 \times 10^{13}$
sr-5m	10	195.3	$5.42 \times 10^{18}$	3	$2.27 \times 10^{13}$
<b>SrF<sub>2</sub></b>					
sr-6	10	478.3	$1.28 \times 10^{19}$	24	$1.16 \times 10^{14}$
sr-7 <sup>b</sup>	10	195.7	$5.25 \times 10^{18}$	43	$1.31 \times 10^{14}$
sr-8m	8	204.5	$5.49 \times 10^{18}$	4	$3.29 \times 10^{13}$
sr-9m	10	314.4	$8.44 \times 10^{18}$	5	$2.77 \times 10^{13}$
<b>SrCO<sub>3</sub></b>					
sr-10	8	91.2	$2.08 \times 10^{18}$	21	$1.64 \times 10^{14}$
sr-11	10	152.1	$3.47 \times 10^{18}$	21	$9.30 \times 10^{13}$
sr-12m	8	222.6	$5.09 \times 10^{18}$	3	$1.91 \times 10^{13}$

<sup>a</sup>Heated at 300°C for 4 h.

<sup>b</sup>Heated at 800°C for 1 h.

### III. DATA ANALYSIS

#### A. General procedure

The induced  $\gamma$ -ray activities were counted after the irradiation in a well defined geometry of  $76.0 \pm 0.5$  mm distance using a shielded HPGe detector in a low background area. Energy and efficiency calibrations have been carried out with a set of reference  $\gamma$ -sources in the energy range between 60 keV and 2000 keV. Fig. 1 shows the  $\gamma$ -ray spectra of the induced activities in the  $^{74}\text{Se}$  and  $^{84}\text{Sr}$  samples.

The total amount of activated nuclei  $Z$  at the end of the irradiation can be deduced from the number of events

$C$  in a particular  $\gamma$ -ray line registered in the HPGe detector during the measuring time  $t_m$  [47]. The factor  $t_w$  corresponds to the waiting time between irradiation and activity measurement.

$$Z = \frac{C(t_m)}{\varepsilon_\gamma I_\gamma k_\gamma (1 - e^{-\lambda t_m}) e^{-\lambda t_w}} \quad (2)$$

The factors  $\varepsilon_\gamma$  and  $I_\gamma$  account for the HPGe efficiency and the relative  $\gamma$  intensity per decay of the respective transition (Table II). The factor  $k_\gamma$  introduces the correction for  $\gamma$ -ray self-absorption in the sample [47]. For disk shaped samples with a thickness  $d$  and  $\gamma$ -ray absorption coefficients  $\mu$  [48], one obtains

$$k_\gamma = \frac{1 - e^{-\mu d}}{\mu d}. \quad (3)$$

The factor

$$f_b = \frac{\int_0^{t_a} \phi(t) e^{-\lambda(t_a-t)} dt}{\int_0^{t_a} \phi(t) dt} \quad (4)$$

accounts for the decay of activated nuclei during the irradiation time  $t_a$  as well as for variations in the neutron flux. This factor can be calculated from the neutron flux history recorded throughout the irradiation with the  $^6\text{Li}$  glass detector in 91 cm distance from the target.

The number of activated nuclei  $Z$  can also be written as

$$Z(i) = N_i \sigma_i \Phi_{tot} f_b(i), \quad (5)$$

where  $\Phi_{tot} = \int \phi(t) dt$  is the time-integrated neutron flux and  $N_i$  the number of atoms in the sample. As our measurements are carried out relative to  $^{197}\text{Au}$  as a standard, the neutron flux  $\Phi_{tot}$  cancels out:

$$\begin{aligned} \frac{Z(i)}{Z(\text{Au})} &= \frac{\sigma_i N_i f_b(i)}{\sigma_{\text{Au}} N_{\text{Au}} f_b(\text{Au})} \\ \Leftrightarrow \sigma_i &= \frac{Z(i) \sigma_{\text{Au}} N_{\text{Au}} f_b(\text{Au})}{Z(\text{Au}) N_i f_b(i)}. \end{aligned} \quad (6)$$

The reference value for the experimental  $^{197}\text{Au}$  cross section in the quasi-stellar spectrum of the  $^7\text{Li}(p,n)^7\text{Be}$  source is  $586 \pm 8$  mb [42]. By averaging the induced activities of the gold foils, one can determine the neutron flux  $\Phi_{tot}$  at the position of the sample and deduce the experimental cross section  $\sigma_i$  of the investigated sample as shown in Eq. 6.

#### B. Ground-state correction

In the case of the activation of  $^{84}\text{Sr}$ , where the neutron capture populates both, ground and isomeric state in  $^{85}\text{Sr}$ , the analyzing procedure is more complicated. While the partial cross section to the isomeric state can be easily calculated as described above, the partial cross

TABLE II: Decay properties of the product nuclei. Shown here are only the strongest transitions, which were considered for analysis. Isotopic abundances are from Ref. [43].

Reaction	Isot. abund. [%]	Final state	Half life	$E_\gamma$ [keV]	$I_\gamma$ [%]	Ref.
$^{74}\text{Se}(n,\gamma)^{75}\text{Se}$	$0.89 \pm 0.04$	Ground state	$119.79 \pm 0.04$ d	136.0	$58.3 \pm 0.7$	[44]
				264.7	$58.9 \pm 0.3$	
$^{84}\text{Sr}(n,\gamma)^{85}\text{Sr}$	$0.56 \pm 0.01$	Ground state	$64.84 \pm 0.02$ d	514.0	$95.7 \pm 4.0$	[45]
		Isomer	$67.63 \pm 0.04$ m	151.2 (EC)	$12.9 \pm 0.7$	
				231.9 (IT)	$84.4 \pm 2.2$	
$^{197}\text{Au}(n,\gamma)^{198}\text{Au}$	100	Ground state	$2.69517 \pm 0.00021$ d	411.8	$95.58 \pm 0.12$	[46]

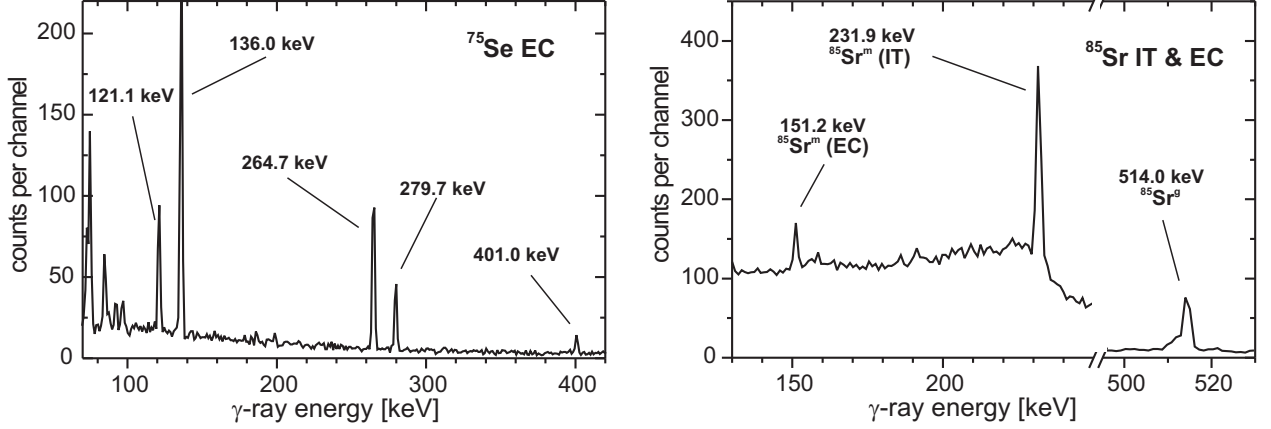


FIG. 1: Decay spectra of the activated Se and Sr samples. The Se spectra shows also the  $\gamma$ -lines at 121 keV, 280 keV and 401 keV, which were not considered for analysis.

section to the ground state has to be corrected for those nuclei, which decayed during activation and measuring time already by isomeric transition.

The amount of isomer and ground state nuclei after the activation time  $t_a$  is described by Eq.7:

$$Z_m(t_a) = N \sigma_m \Phi_{tot} f_m^b \quad (7)$$

$$Z_g(t_a) = N \Phi_{tot} (\sigma_g f_g^b + Y \sigma_m \lambda_m g_m). \quad (8)$$

$Y$  is the branching ratio of the isomeric transition (0.866 for  $^{85}\text{Sr}^m$ ), and the factor  $g_m$  is calculated with:

$$g_m = \frac{\int_0^{t_a} e^{-\lambda_g(t_a-t)} dt \int_0^t \phi(t^*) e^{-\lambda_m(t-t^*)} dt^*}{\int_0^{t_a} \phi(t) dt}. \quad (9)$$

The relation between the activity of the ground state and the measured count rate  $C_g$  can be calculated by

$$C_g(t_w + t_m) = k_\gamma \varepsilon_\gamma I_\gamma \int_{t_w}^{t_w+t_m} A_g(t) dt. \quad (10)$$

$A_g(t)$  is further described as

$$A_g(t) = A_g(t_a) e^{-\lambda_g t} + Y \frac{\lambda_g}{\lambda_g - \lambda_m} A_m(t_a) (e^{-\lambda_m t} - e^{-\lambda_g t}). \quad (11)$$

Inserting  $A_i = Z_i \lambda_i$ , solving the integral and converting to  $Z_g(t_a)$  leads to

$$Z_g(t_a) = \frac{C(t_w + t_m)}{k_\gamma \varepsilon_\gamma I_\gamma (e^{-\lambda_g t_w} - e^{-\lambda_g(t_w+t_m)})} - \frac{Y \frac{\lambda_g}{\lambda_g - \lambda_m} Z_m(t_a) (e^{-\lambda_m t_w} - e^{-\lambda_m(t_w+t_m)})}{e^{-\lambda_g t_w} - e^{-\lambda_g(t_w+t_m)}} + \frac{Y \frac{\lambda_m}{\lambda_g - \lambda_m} Z_m(t_a) (e^{-\lambda_g t_w} - e^{-\lambda_g(t_w+t_m)})}{e^{-\lambda_g t_w} - e^{-\lambda_g(t_w+t_m)}}. \quad (12)$$

Thus,  $\sigma_g$  can finally be deduced from Eq. 8 by inserting  $Z_g(t_a)$ :

$$\sigma_g = \frac{Z_g(t_a)}{N \Phi_{tot} f_g^b} - \frac{Y \sigma_m \lambda_m g_m}{f_g^b}. \quad (13)$$

The second term in Eq. 13 describes the isomeric transition, for which the ground-state cross section has to be corrected. For half-lives longer than the ground-state, this part introduces major corrections, whereas for very short half-lives this term becomes negligible.

## IV. RESULTS AND DISCUSSION

### A. General

In an astrophysical environment with temperature  $T$ , the neutron spectrum corresponds to a Maxwell-Boltzmann distribution

$$\Phi \sim E_n e^{-E_n/kT}. \quad (14)$$

The experimental neutron spectrum of the  ${}^7\text{Li}(p,n){}^7\text{Be}$  reaction approximates a Maxwellian distribution with  $kT=25$  keV almost perfectly [42]. But to obtain the exact Maxwellian averaged cross section  $\langle\sigma\rangle_{kT}=\frac{\langle\sigma v\rangle}{v_T}$  for the temperature  $T$ , the energy-dependent cross section  $\sigma(E)$  has to be folded with the experimental neutron distribution to derive a normalization factor  $\text{NF}=\frac{\sigma}{\sigma_{exp}}$ . The region beyond the resonances (2.4 keV for  ${}^{74}\text{Se}$  and 3.5 keV for  ${}^{84}\text{Sr}$ ) was then multiplied with the normalization factor NF. The proper Maxwellian averaged cross section as a function of thermal energy  $kT$  was then derived from the normalized cross section (Fig. 2) in the energy range  $0.01\leq E_n\leq 4000$  keV.

$$\frac{\langle\sigma v\rangle}{v_T} = \langle\sigma\rangle_{kT} = \frac{2}{\sqrt{\pi}} \frac{\int_0^\infty \frac{\sigma(E_n)}{\text{NF}} E_n e^{-E_n/kT} dE_n}{\int_0^\infty E_n e^{-E_n/kT} dE_n}. \quad (15)$$

In this equation,  $\frac{\sigma(E_n)}{\text{NF}}$  is the normalized energy-dependent capture cross section and  $E_n$  the neutron energy. The factor  $v_T=\sqrt{2kT/m}$  denotes the most probable velocity with the reduced mass  $m$ .

For astrophysical applications, laboratory cross sections have to be converted to stellar cross sections involving thermally excited targets by applying a correction factor, the so-called stellar enhancement factor (SEF) [12]. While there are only comparatively few cases with low-lying nuclear states in the  $s$  process where the correction is important, it is to be expected that the SEF may be larger at the much higher  $p$ -process temperatures. However, this is not the case for the  $p$  nuclei considered here, as illustrated by Table III.

TABLE III: Stellar enhancement factors for different temperatures [12].

T [GK]	$kT$ [keV]	SEF( ${}^{74}\text{Se}$ )	SEF( ${}^{84}\text{Sr}$ )
0.3	26	1.00	1.00
2.0	172	1.01	1.02
2.5	215	1.02	1.06
3.0	260	1.03	1.09

For  ${}^{74}\text{Se}$  and  ${}^{84}\text{Sr}$ , energy-dependent neutron capture cross sections were available from JEFF 3.0 [49], ENDF-B VI.8 [50], and NON-SMOKER [12, 13, 51], whereas JENDL 3.3 [52] provides only data for  ${}^{74}\text{Se}$ . The energy region between 10 eV and 2.9 keV in JEFF, ENDF-B and JENDL includes experimentally evaluated

data [53] and differs only in the strength of the resonances. The trend beyond 2.9 keV is deduced from statistical model calculations and deviates from NON-SMOKER when the  $(n,p)$  channel opens at  $E_n>600$  keV ( ${}^{74}\text{Se}$ ) and  $E_n>750$  keV ( ${}^{84}\text{Sr}$ ), respectively. In the following sections we will use the energy dependencies of JEFF 3.0 to determine Maxwellian averaged cross sections and compare the results only with NON-SMOKER.

### B. Uncertainties

The experimental uncertainties are summarized in Table IV. Since nearly every stellar neutron cross section measurement was carried out relative to gold, the error of 1.4% [42] in the gold cross section cancels out.

Uncertainties between 1.4% (for samples with 10 mm diameter) and 2.9% (6 mm diameter) are due to an estimated sample position uncertainty of 0.25 mm relative to the Au foils during the activation, which affects neutron flux seen by the sample. For the Se samples, a fairly large contribution results from the 4.5% error of the isotopic abundance [43]. In the case of the  ${}^{84}\text{Sr}(n,\gamma){}^{85}\text{Sr}^{g+m}$  capture cross sections, considerable contributions come from the uncertainties of the  $\gamma$ -ray intensities. The errors in the time factors  $f_b$ ,  $f_w=e^{-\lambda t_w}$  and  $f_m=e^{-\lambda t_m}$  are negligible in all measurements except those of the partial cross section to  ${}^{85}\text{Sr}^m$  ( $t_{1/2}=67.6$  m) due to the rather long half-lives of the product nuclei in comparison with  $t_w$  and  $t_m$ . The error in the masses could be neglected for all samples except for the gold foils.

TABLE IV: Compilation of uncertainties.

Source of uncertainty	Uncertainty (%)			
	${}^{197}\text{Au}$	${}^{74}\text{Se}$	${}^{84}\text{Sr}\rightarrow g$	${}^{84}\text{Sr}\rightarrow m$
Gold cross section	1.4 <sup>a</sup>	-	-	-
Isotopic abundance	-	4.5	1.8	1.8
Detector efficiency	1.5	1.5	1.5	1.5
Divergence of n flux	-	1.4 - 2.3	1.5 - 2.9	1.5 - 2.9
Sample mass	0.2	-	-	-
$\gamma$ -Ray intensity	0.1	0.5/ 1.2 <sup>b</sup>	4.2 <sup>c</sup>	5.4/ 2.6 <sup>d</sup>
$\gamma$ -Ray self-absorption	-	0.2	0.2	0.2
Counting statistics	1.0	0.4 - 1.6	3.6 - 5.3	0.4 - 2.0
Time factors $f_b$ , $f_m$ , $f_w$	-	-	-	0.2 - 1.3
Total uncertainty		5.5 - 5.7 <sup>e</sup>	6.5 - 7.9 <sup>e</sup>	4.3 - 7.1 <sup>e</sup>

<sup>a</sup>Not included in the final uncertainty, see text.

<sup>b</sup>136 keV/ 265 keV.

<sup>c</sup>514 keV

<sup>d</sup>151 keV/ 232 keV.

<sup>e</sup>Incl. uncertainty from Au.

The conservatively assumed overall uncertainty for the Se measurements is 5.7%. The partial cross sections to the  ${}^{85}\text{Sr}$  ground and isomeric states have uncertainties of 7.1% and 5.3%, respectively, leading to a combined error of 5.6% in the total capture cross section. These uncertainties were also adopted for the Maxwellian av-

eraged cross sections, assuming that the uncertainties of the theoretical energy dependence were negligible for the extrapolation to  $kT=30$  keV.

### C. $^{74}\text{Se}(n,\gamma)^{75}\text{Se}$

The  $^{74}\text{Se}(n,\gamma)^{75}\text{Se}$  reaction was analyzed via the two strongest transitions in  $^{75}\text{As}$  at 136.0 keV and 264.7 keV. The results from the individual Se activations are listed in Table V. The capture cross section derived with the experimental neutron distribution is  $281\pm 16$  mb and was calculated as the weighted mean value of all five activations.

TABLE V: Results from the Se activations.

Activation $^{74}\text{Se}(n,\gamma)^{75}\text{Se}$	Cross section [mb]	
	(136 keV)	(265 keV)
se-1	$283 \pm 16$	$276 \pm 16$
se-2	$270 \pm 15$	$259 \pm 14^a$
se-3	$273 \pm 16$	$265 \pm 15$
se-4	$291 \pm 16$	$287 \pm 16$
se-5	$300 \pm 17$	$284 \pm 16$
Mean cross section	$281 \pm 16$	

<sup>a</sup>Value not included in mean value.

### D. $^{84}\text{Sr}(n,\gamma)^{85}\text{Sr}$

In case of  $^{84}\text{Sr}$ , neutron captures populate both, ground and isomeric state of  $^{85}\text{Sr}$ . While  $^{85}\text{Sr}^g$  decays can be identified via the 514 keV transition in  $^{85}\text{Rb}$ , the decay of the isomer proceeds mainly via transitions of 232 keV and 151 keV. The isomeric state is 239 keV above the ground state and decays either via a 7 keV- 232 keV cascade (internal transition, 86.6%) or directly by electron capture (13.4%) into the 151 keV level of the daughter nucleus  $^{85}\text{Rb}$ .

The partial cross section to the isomeric state can be easily deduced from the above mentioned transitions at 151 keV and 232 keV and yields  $189\pm 10$  mb (see Table VI). The cross section to the ground state has to be corrected for the internal decay of the isomer during the activation and measuring time, and results in  $112\pm 8$  mb. This leads to a total capture cross section of  $301\pm 18$  mb.

The corresponding isomeric ratio is  $IR=0.63\pm 0.04$ , in perfect agreement with the value of  $0.63\pm 0.06$  reported for thermal neutrons [54]. A NON-SMOKER estimation showed that the isomeric ratio is almost independent of the energy  $kT$  in the relevant range.

TABLE VI: Results from the Sr activations.

Activation $^{84}\text{Sr}(n,\gamma)$	cross section [mb]		
	$\rightarrow^{85}\text{Sr}^g$	$\rightarrow^{85}\text{Sr}^m$	
	(514 keV)	(151 keV)	(232 keV)
sr-1	$114 \pm 9$		
sr-2	$124 \pm 8$		
sr-3	$102 \pm 8$		
sr-4m		$189 \pm 13$	$194 \pm 10$
sr-5m		$194 \pm 13$	$194 \pm 8$
sr-6	$106 \pm 7$	$178 \pm 12$	$189 \pm 8$
sr-7	$107 \pm 7$		
sr-8m		$186 \pm 12$	$190 \pm 9$
sr-9m		$187 \pm 12$	$191 \pm 8$
sr-10	$122 \pm 8$	$192 \pm 13$	$192 \pm 9$
sr-11	$106 \pm 7$		
sr-12m		$178 \pm 12$	$189 \pm 9$
Mean cross section	$112 \pm 8$	$189 \pm 10$	

## V. COMPARISON WITH THEORY

### A. Maxwellian cross sections for $kT=25$ keV

$^{74}\text{Se}(n,\gamma)$ : Normalization of the energy dependent cross sections  $\sigma(E_n)$  from NON-SMOKER, JEFF 3.0, ENDF-B VI.8 and JENDL 3.3 with the experimental value of 281 mb yields normalization factors between 0.568 and 0.736 (see Table VII). Fig. 2 shows the normalized  $\sigma(E)$  spectra for JEFF and NON-SMOKER in comparison with the original spectra. The Maxwellian averaged cross section at  $kT=25$  keV deduced with the JEFF dependence is  $\langle\sigma\rangle_{25}=298$  mb.

$^{84}\text{Sr}(n,\gamma)$ : The normalization factors for  $^{84}\text{Sr}$  vary between 0.774 and 1.076 (Table VII). With the normalized spectra of JEFF (Fig. 2) the resulting total stellar capture cross section  $\langle\sigma\rangle_{25}(\text{total})$  is 326 mb. With our isomeric ratio of 0.63 we calculate for the partial cross section to the isomer  $^{85}\text{Sr}^m$   $\langle\sigma\rangle_{25}(\text{part})=205$  mb.

TABLE VII: Cross sections derived by folding the experimental neutron distribution with the  $\sigma(E)$  data of different libraries. NF denotes the respective normalization factors compared to the experimental cross section.

	$^{74}\text{Se}$		$^{84}\text{Sr}$	
	cross section	NF	cross section	NF
Experiment	281 mb	1.000	301 mb <sup>a</sup>	1.000
JEFF 3.0	160 mb	0.568	234 mb <sup>a</sup>	0.779
ENDF-B VI.8	160 mb	0.568	233 mb <sup>a</sup>	0.774
JENDL 3.3	207 mb	0.736	-	-
NON-SMOKER	206 mb	0.731	324 mb <sup>a</sup>	1.076

<sup>a</sup>Total capture cross section

## B. Extrapolation to higher temperatures

Table IX shows the Maxwellian averaged cross sections for different thermal energies deduced with JEFF. The respective reaction rates were calculated from  $\langle\sigma\rangle_{kT}$  via

$$N_A < \sigma v > = 26445.5 < \sigma >_{kT} \sqrt{kT/m} \quad (16)$$

with  $m$  being the reduced mass. The units for  $\langle\sigma\rangle_{kT}$ , the thermal energy  $kT$  and the reaction rate  $N_A < \sigma v >$  are [mb], [keV] and [ $\text{mole}^{-1} \text{cm}^3 \text{s}^{-1}$ ], respectively. By convention, stellar neutron capture rates for  $s$ -process studies are compared at  $kT = 30$  keV, which corresponds also to the freeze-out temperature of  $3.5 \times 10^8$  K. For  $p$ -process applications, the cross sections should be extrapolated to the energy range, which is relevant for the  $p$  process, i.e.  $170 \text{ keV} \leq kT \leq 260 \text{ keV}$ , corresponding to temperatures of  $(2 \text{ to } 3) \times 10^9$  K.

For  $^{74}\text{Se}$  a Maxwellian averaged cross section of  $\langle\sigma\rangle_{30} = 271$  mb is derived, in perfect agreement with the previously estimated value of  $267 \pm 25$  mb from Ref. [41]. The result for  $^{84}\text{Sr}$  is  $\langle\sigma\rangle_{30}(\text{tot}) = 300$  mb, 18% lower than the  $368 \pm 125$  mb from Ref. [41]. The partial cross section to the isomer yields  $\langle\sigma\rangle_{30}(\text{part}) = 190$  mb.

Fig. 3 shows theoretical predictions for the  $\langle\sigma\rangle_{30}$  values of  $^{74}\text{Se}$  [13, 14, 15, 41, 55, 56, 57, 58] and  $^{84}\text{Sr}$  [13, 14, 15, 41, 55, 57, 58, 59] in comparison with our experimental value. In the case of  $^{74}\text{Se}$  agreement is only found with the old and new MOST predictions [14, 15] and with the normalized NON-SMOKER cross sections in [41], which account for known systematic deficiencies in the nuclear inputs of the calculation. For  $^{84}\text{Sr}$ , older predictions from Refs. [55, 57, 59] are in rather good agreement. Not shown in this plot is a corrected prediction from the old MOST code of 2002 [60] of 296 mb, which was also in good agreement with our experimental Maxwellian cross section at  $kT = 30$  keV. Table VIII gives a comparison between the two Hauser-Feshbach models MOST (with the versions of 2002 [14] and 2005 [15]) and NON-SMOKER, and the previous recommended (semi-empirical) value from Ref. [41]. A full list of all 32  $p$  nuclei can be found in [61].

Further extrapolation to temperatures between  $kT = 5$  keV and 260 keV (Fig. 4) shows the different energy dependence of the data based on the NON-SMOKER, JEFF and MOST predictions. For this plot, the curves of NON-SMOKER and MOST were normalized to the JEFF values at  $kT = 25$  keV. In the case of  $^{74}\text{Se}$  the data libraries deviate at low and agree at higher energies, whereas  $^{84}\text{Sr}$  exhibits an opposite trend. The results for the Maxwellian averaged cross sections at  $p$ -process temperatures are  $\langle\sigma\rangle_{260} = 115$  mb for  $^{74}\text{Se}$  and 161 mb for  $^{84}\text{Sr}$ , corresponding to stellar reaction rates of  $4.92 \times 10^7$  and  $6.91 \times 10^7 \text{ mole}^{-1} \text{cm}^3 \text{s}^{-1}$ , respectively. The temperature trends of the reaction rates are shown in Fig. 5.

TABLE VIII: Present Maxwellian averaged cross sections  $\langle\sigma\rangle_{30}$  at  $kT = 30$  keV compared to the Hauser-Feshbach calculations MOST and NON-SMOKER and data in [41].

$^{74}\text{Se}$	Source	$\langle\sigma\rangle_{30}$ [mb]	Reference
	NON-SMOKER	207	[13]
	MOST 2002	304	[14]
	MOST 2005	247	[15]
	Bao et al.	$267 \pm 25$	[41]
	This work	$271 \pm 15$	
$^{84}\text{Sr}$	Source	$\langle\sigma\rangle_{30}$ [mb] <sup>a</sup>	Reference
	NON-SMOKER	393	[13]
	MOST 2002	$74^b$	[14]
	MOST 2005	246	[15]
	Bao et al.	$368 \pm 125$	[41]
	This work	$300 \pm 17$	

<sup>a</sup> Total capture cross section.

<sup>b</sup> Original value. Corrected value [60] is 296 mb for  $^{84}\text{Sr}$ .

TABLE IX: Maxwellian averaged cross sections and reaction rates (including SEF from Table III) for thermal energies between  $kT = 5$  keV and 260 keV derived with the energy dependence of JEFF 3.0.

kT [keV]	$^{74}\text{Se}$		$^{84}\text{Sr}$	
	$\langle\sigma\rangle_{kT}$ [mb]	$N_A < \sigma v >$ [ $\text{mole}^{-1} \text{cm}^3 \text{s}^{-1}$ ]	$\langle\sigma\rangle_{kT}^a$ [mb]	$N_A < \sigma v >$ [ $\text{mole}^{-1} \text{cm}^3 \text{s}^{-1}$ ]
5	775	$4.61 \times 10^7$	683	$4.07 \times 10^7$
10	500	$4.21 \times 10^7$	499	$4.20 \times 10^7$
15	395	$4.08 \times 10^7$	413	$4.25 \times 10^7$
20	337	$4.01 \times 10^7$	361	$4.30 \times 10^7$
25	298	$3.97 \times 10^7$	326	$4.33 \times 10^7$
30	271	$3.95 \times 10^7$	300	$4.37 \times 10^7$
40	233	$3.93 \times 10^7$	264	$4.44 \times 10^7$
50	209	$3.94 \times 10^7$	240	$4.52 \times 10^7$
60	192	$3.97 \times 10^7$	224	$4.61 \times 10^7$
80	170	$4.06 \times 10^7$	201	$4.79 \times 10^7$
100	157	$4.17 \times 10^7$	187	$4.99 \times 10^7$
170	133	$4.60 \times 10^7$	167	$5.79 \times 10^7$
215	123	$4.79 \times 10^7$	164	$6.41 \times 10^7$
260	115	$4.92 \times 10^7$	161	$6.91 \times 10^7$

<sup>a</sup>Total capture cross section

## VI. SUMMARY AND OUTLOOK

We have presented the first results of an ongoing experimental program to determine more precise  $p$ -process reaction rates in the mass range  $A = 70$ -140. The stellar  $(n, \gamma)$  cross sections of the  $p$  nuclei  $^{74}\text{Se}$  and  $^{84}\text{Sr}$  have been measured for the first time, yielding values of 281 mb for  $^{74}\text{Se}$ , and 112 mb for the ground and 189 mb for the isomeric state to  $^{85}\text{Sr}$  with our experimental neutron spectrum. The respective Maxwellian averaged cross sections for  $kT = 30$  keV were derived with the energy dependence of JEFF 3.0 and result in  $\langle\sigma\rangle_{30} = 271 \pm 15$  mb for  $^{74}\text{Se}$ , and  $\langle\sigma\rangle_{30}(\text{total}) = 300 \pm 17$  mb for  $^{84}\text{Sr}$ . The isomeric ratio IR was found to be  $0.63 \pm 0.04$  and thus yields a partial stellar cross section

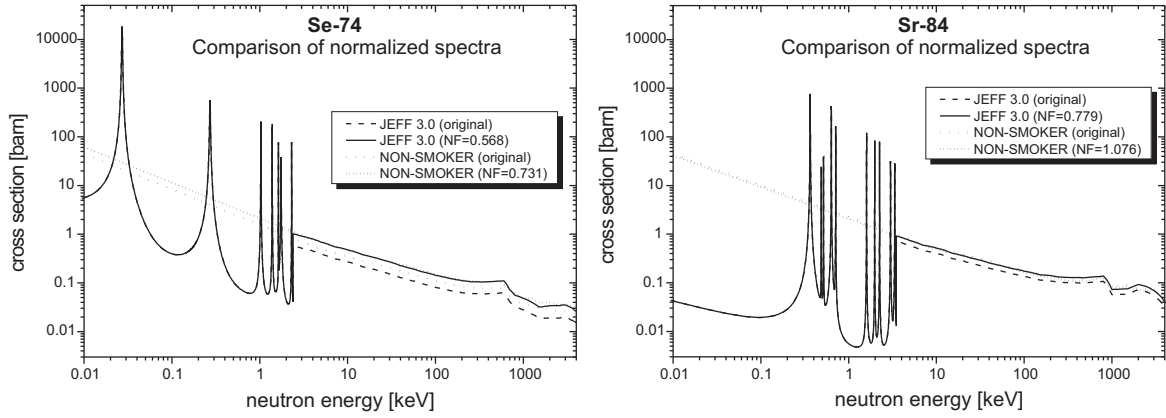


FIG. 2: Energy-dependent cross sections  $\sigma(E)$  for  $^{74}\text{Se}$  and  $^{84}\text{Sr}$ , predicted by JEFF 3.0 and NON-SMOKER. Shown are the original data in comparison with the normalized data. Since the resonances in both cases are experimentally, only the curve beyond this region was normalized to our experimental value.

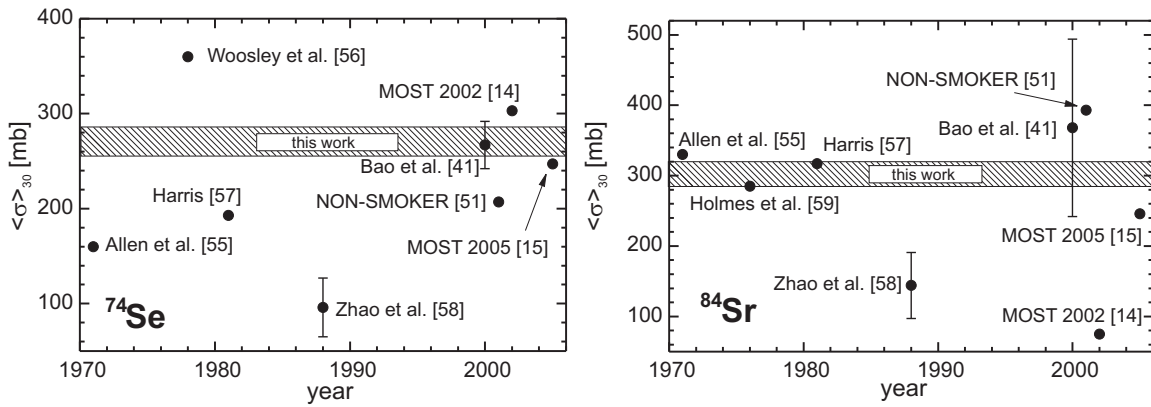


FIG. 3: Comparison of theoretically predicted Maxwellian averaged cross sections  $\langle\sigma\rangle_{30}$  and the experimental values (derived with the energy dependence of JEFF 3.0) for  $^{74}\text{Se}$  and  $^{84}\text{Sr}$ .

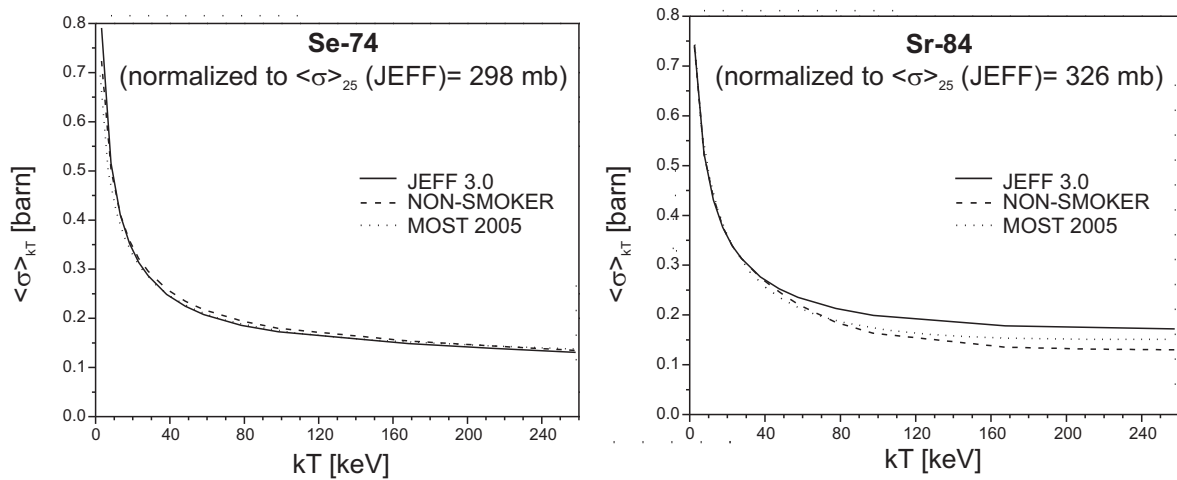


FIG. 4: Temperature dependence of Maxwellian averaged cross sections derived by normalizing different predicted cross sections to the value deduced with JEFF 3.0 at  $kT=25$  keV.



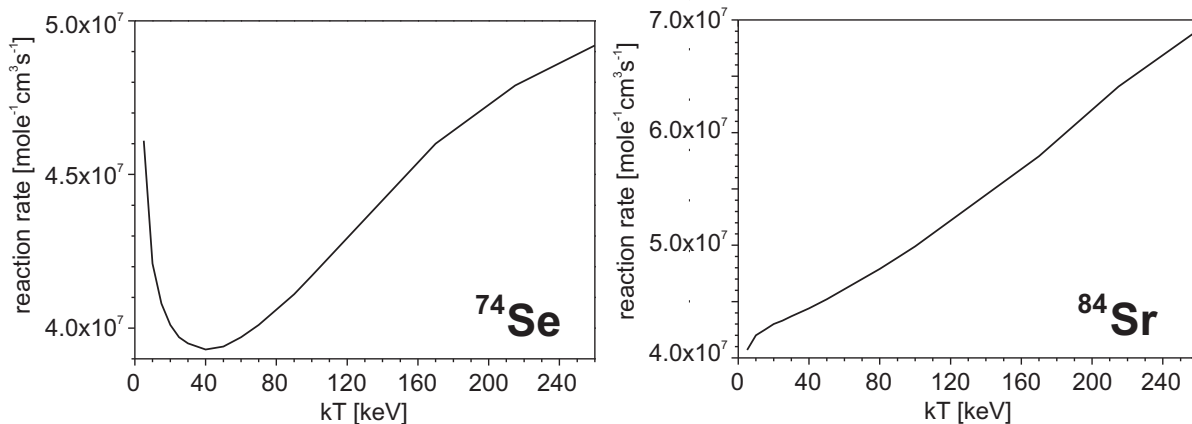


FIG. 5: Temperature trend of the reaction rates for  $^{74}\text{Se}$  and  $^{84}\text{Sr}$  derived with the normalized energy-dependent cross sections of JEFF 3.0 (see Table IX).

of  $\langle \sigma \rangle_{30(\text{part.})} = 190 \pm 10$  mb.

Over the past decade, a lot of work has been devoted to measure cross sections and reaction rates of  $p$  nuclei, but experimental ( $p, \gamma$ ), ( $\alpha, \gamma$ ) and photodisintegration rates are still very scarce. The situation for stellar ( $n, \gamma$ ) cross sections is somewhat better, but it should be pointed out that nearly all of the ( $n, \gamma$ ) measurements were performed in energy regions relevant for the  $s$  process ( $kT = 30$  keV instead of  $100 < kT < 260$  keV for the  $p$  process), whereas the charged particle rates are measured close to the respective  $p$ -process Gamow window.

The measurements presented in this paper mark the beginning of an extensive experimental program to determine more precise neutron cross sections of stable  $p$  nuclei. Within this program, we have already finished the measurement on  $^{96}\text{Ru}$  [35], and preliminary values

are available for  $^{102}\text{Pd}$ ,  $^{120}\text{Te}$ ,  $^{130}\text{Ba}$ ,  $^{132}\text{Ba}$  and  $^{174}\text{Hf}$  [61]. All available experimental information will be summarized in an upcoming paper, including an extrapolation to the full range of  $p$ -process temperatures and the calculation of inverse reaction rates by detailed balance.

#### Acknowledgments

We thank E. P. Knaetsch, D. Roller and W. Seith for their help and support during the irradiations at the Van de Graaff accelerator. This work was supported by the Swiss National Science Foundation Grants 2024-067428.01 and 2000-105328.

- 
- [1] E. Burbidge, G. Burbidge, W. Fowler, and F. Hoyle, *Rev. Mod. Phys.* **29**, 547 (1957).  
 [2] K. Langanke and M. Wiescher, *Rep. Prog. Phys.* **64**, 1657 (2001).  
 [3] S. Woosley and W. Howard, *Ap. J. Suppl.* **36**, 285 (1978).  
 [4] S. Woosley and W. Howard, *Ap. J.* **354**, L21 (1990).  
 [5] M. Rayet, M. Arnould, M. Hashimoto, N. Prantzos, and K. Nomoto, *Astron. Astrophys.* **298**, 517 (1995).  
 [6] T. Rauscher, A. Heger, R. Hoffman, and S. Woosley, *Ap. J.* **576**, 323 (2002).  
 [7] W. Howard, B. Meyer, and S. Woosley, *Ap. J.* **373**, L5 (1991).  
 [8] H. Schatz, A. Aprahamian, J. Görres, M. Wiescher, T. Rauscher, J. Rembges, F.-K. Thielemann, B. Pfeiffer, P. Möller, H. Herndl, et al., *Phys. Rep.* **294**, 167 (1998).  
 [9] M. Arnould and S. Goriely, *Phys. Rep.* **384**, 1 (2003).  
 [10] W. Hauser and H. Feshbach, *Phys. Rev.* **87**, 366 (1952).  
 [11] T. Rauscher, F.-K. Thielemann, and H. Oberhummer, *Ap. J.* **451**, L37 (1995).  
 [12] T. Rauscher and F.-K. Thielemann, *ADNDT* **75**, 1 (2000).  
 [13] T. Rauscher and F.-K. Thielemann, *ADNDT* **79**, 47 (2001).  
 [14] S. Goriely, Hauser-Feshbach rates for neutron capture reactions (version 09/12/02), <http://www-astro.ulb.ac.be/Html/hfr.html> (2002).  
 [15] S. Goriely, Hauser-Feshbach rates for neutron capture reactions (version 08/26/05), <http://www-astro.ulb.ac.be/Html/hfr.html> (2005).  
 [16] T. Rauscher, *Nucl. Phys. A* **758**, 549c (2005).  
 [17] W. Rapp, Report FZKA 6956, Forschungszentrum Karlsruhe (2004).  
 [18] M. Rayet, N. Prantzos, and M. Arnould, *Astron. Astrophys.* **227**, 271 (1990).  
 [19] P. Mohr, K. Vogt, M. Babilon, J. Enders, T. Hartmann, C. Hutter, T. Rauscher, S. Volz, and A. Zilges, *Phys. Lett. B* **488**, 127 (2000).  
 [20] K. Vogt, P. Mohr, M. Babilon, J. Enders, T. Hartmann, C. Hutter, T. Rauscher, S. Volz, and A. Zilges, *Phys. Rev. C* **63**, 055802 (2001).  
 [21] H. Utsunomiya, H. Akimune, S. Goko, T. Hayakawa, Y.-

- W. Lui, H. Ohgaki, M. Ohta, T. Shizuma, H. Toyokawa, and T. Yamagata, Nucl. Phys. A **718**, 199c (2003).
- [22] H. Utsunomiya, H. Akimune, S. Goko, M. Ohta, H. Ueda, T. Yamagata, K. Yamasaki, H. Ohgaki, H. Toyokawa, Y.-W. Lui, et al., Phys. Rev. C **67**, 015807 (2003).
- [23] K. Sonnabend, P. Mohr, K. Vogt, A. Zilges, A. Mengoni, T. Rauscher, H. Beer, F. Käppeler, and R. Gallino, Ap. J. **583**, 506 (2003).
- [24] K. Sonnabend, K. Vogt, D. Galaviz, S. Müller, and A. Zilges, Phys. Rev. C **70**, 035802 (2004).
- [25] T. Rauscher and F.-K. Thielemann, ADNDT **88**, 1 (2004).
- [26] Z. Fülöp, A. Kiss, E. Somorjai, C. Rolfs, H.-P. Trautvetter, T. Rauscher, and H. Oberhummer, Z. Phys. A **355**, 203 (1996).
- [27] T. Sauter and F. Käppeler, Phys. Rev. C **55**, 3127 (1997).
- [28] E. Somorjai, Z. Fülöp, A. Kiss, C. Rolfs, H.-P. Trautvetter, U. Greife, M. Junker, M. Arnould, M. Rayet, S. Goriely, et al., Astron. Astrophys. **333**, 1112 (1998).
- [29] E. Somorjai, Z. Fülöp, A. Kiss, C. Rolfs, H.-P. Trautvetter, U. Greife, M. Junker, M. Arnould, M. Rayet, S. Goriely, et al., Proc. Nuclei in the Cosmos V, eds. N. Prantzos and S. Harissopulos, Editions Frontières p. 459 (1998).
- [30] J. Bork, H. Schatz, F. Käppeler, and T. Rauscher, Phys. Rev. C **58**, 524 (1998).
- [31] F. Chloupek, A. Murphy, R. Boyd, A. Cole, J. Görres, R. Guray, G. Raimann, J. Zach, T. Rauscher, J. Schwarzenberg, et al., Nucl. Phys. A **652**, 391 (1999).
- [32] S. Harissopulos, E. Skreti, P. Tsagari, G. Souliotis, P. Demetriou, T. Paradellis, J. Hammer, R. Kunz, C. Angulo, S. Goriely, et al., Phys. Rev. C **64**, 055804 (2001).
- [33] G. Gyürky, E. Somorjai, Z. Fülöp, S. Harissopulos, P. Demetriou, and T. Rauscher, Phys. Rev. C **64**, 065803 (2001).
- [34] N. Özkan, A. Murphy, R. Boyd, A. Cole, M. Famiano, M. Howard, L. Sahin, J. Zach, R. de Haan, J. Görres, et al., Nucl. Phys. A **710**, 469 (2002).
- [35] W. Rapp, M. Heil, D. Hentschel, F. Käppeler, R. Reifarth, H.J. Brede, H. Klein, and T. Rauscher, Phys. Rev. C **66**, 015803 (2002).
- [36] S. Galanopoulos, P. Demetriou, M. Kokkoris, S. Harissopulos, R. Kunz, M. Fey, J. Hammer, G. Gyürky, E. Somorjai, Z. Fülöp, et al., Phys. Rev. C **67**, 015801 (2003).
- [37] G. Gyürky, Z. Fülöp, E. Somorjai, M. Kokkoris, S. Galanopoulos, P. Demetriou, S. Harissopulos, T. Rauscher, and S. Goriely, Phys. Rev. C **68**, 055803 (2003).
- [38] S. Harissopulos, S. Galanopoulos, P. Demetriou, A. Syrou, G. Kriembardis, M. Kokkoris, A. Karydas, C. Zarkardas, R. Kunz, R., et al., Nucl. Phys. A **719**, 115c (2003).
- [39] K. Wisshak, F. Voss, C. Theis, F. Käppeler, K. Guber, L. Kazakov, N. Kornilov, and G. Reffo, Phys. Rev. C **54**, 1451 (1996).
- [40] C. Theis, F. Käppeler, K. Wisshak, and F. Voss, Ap. J. **500**, 1039 (1998).
- [41] Z. Bao, H. Beer, F. Käppeler, F. Voss, K. Wisshak, and T. Rauscher, ADNDT **76**, 70 (2000).
- [42] W. Ratynski and F. Käppeler, Phys. Rev. C **37**, 595 (1988).
- [43] K. Rosman and P. Taylor, Pure and Appl. Chem. **70**, 217 (1998).
- [44] A. Farhan and B. Singh, Nucl. Data Sheets **86**, 785 (1999).
- [45] H. Sievers, Nucl. Data Sheets **62**, 271 (1991).
- [46] Z. Chunmei, Nucl. Data Sheets **95**, 59 (2002).
- [47] H. Beer and F. Käppeler, Phys. Rev. C **21**, 534 (1980).
- [48] J. Hubbell and S. Seltzer, Table of X-Ray Mass Attenuation Coefficients and Mass Energy-Absorption Coefficients (v. 1.4), National Institute of Standards and Technology, Gaithersburg, MD ; <http://physics.nist.gov/PhysRefData/XrayMassCoef/> (2004).
- [49] NEA, Joint Evaluated Fission and Fusion General Purpose File: JEFF 3.0; Online: [www.nea.fr/html/dbdata/eva/evaret.cgi](http://www.nea.fr/html/dbdata/eva/evaret.cgi) (2004).
- [50] NNDC, National Nuclear Data Center, Brookhaven NH: ENDF/B-VI Release 8; Online: [www.nndc.bnl.gov/exfor1/endlf00.htm](http://www.nndc.bnl.gov/exfor1/endlf00.htm) (2004).
- [51] T. Rauscher, HTML Interface NON-SMOKER; Online: <http://nucastro.org/nosmo.html> (2001).
- [52] K. Shibata, T. Kawano, and T. Nakagawa, Japanese Evaluated Nuclear Data Library Version 3 Revision 3: JENDL 3.3, J. Nucl. Sci. Technol. **39**, 1125 (2002).
- [53] S. Sukhoruchkin, Z. Soroko, and V. Deriglazov, Landolt-Börnstein, Group I: Elementary Particles, Nuclei and Atoms, Vol. 16; Low Energy Neutron Physics - Subvolume B; edited by H. Schopper (1998).
- [54] S. Mughabghab, M. Divadeenam, and N. Holden, Neutron Cross Sections, BNL-325, 1st ed., **1** (1981).
- [55] B. Allen, J. Gibbons, and R. Macklin, Adv. Nucl. Phys. **4**, 205 (1971).
- [56] S. Woosley, W. Fowler, J. Holmes, and B. Zimmerman, ADNDT **22**, 371 (1978).
- [57] M. Harris, Astrophys. Space Sci. **77**, 357 (1981).
- [58] Z. Zhao, D. Zhou, and D. Cai, Nuclear Data for Science and Technology, eds. S. Igarasi (Saikon, Tokyo) p. 513 (1988).
- [59] J. Holmes, S. Woosley, W. Fowler, and B. Zimmerman, ADNDT **18**, 305 (1976).
- [60] S. Goriely, private comm. (2005).
- [61] I. Dillmann, M. Heil, F. Käppeler, R. Plag, T. Rauscher, and F.-K. Thielemann, Proceedings of the 12th Int. Conference on Capture Gamma-Ray Spectroscopy and Related Topics, Notre Dame/USA, Sept. 4-9, 2005, to be published by AIP (2005).